Glycosylation-Enhanced Luminescence of Nonaromatic Amino Acids

Qiang Zhang, Zihao Zhao, Guangxin Yang, Anze Li, Yijing Cui, Yusong Cai, Zhuojie Yin, Yuntian Tan, Chenyang Zhou, Qian Peng, and Wang Zhang Yuan*

KEYWORDS**:** *nonaromatic amino acids, sugars, glycosylation, nonconventional luminophores, autofluorescence, room temperature phosphorescence*

ABSTRACT: Nonaromatic amino acids with intrinsic photoluminescence (PL) have drawn growing attention due to their crucial role in the luminescence of natural proteins. Nevertheless, the faint luminescence significantly constrains the mechanism exploration of biomolecules as well as their practical applications. We here report a serendipitous finding of synergetic PL enhancement by coupling both weakly emissive nonaromatic amino acids and sugars via glycosidic bonds. Namely, glycosylation drastically boosted the quantum yields of nonaromatic amino acids from 0.3% to as high as 9.2%, accompanied by the emergence of pronounced persistent room temperature phosphorescence (p-RTP). This synergistic PL enhancement arises from the ingenious integration of the electron-rich oxygen clusters present in sugar with the charge separation characteristics of amino acids. Driven by amino acids, ample electrons supplied by the sugar rings are directionally induced to promote electron delocalization, as well as subsequently enhanced absorption, resulting in a more efficient excitation process. Furthermore, the ultrafast femtosecond to nanosecond transient absorption (fs-TA, ns-TA) spectroscopy and theoretical calculations further reveal the importance of hybridization of the locally excited (LE) and the charge transfer (CT) states for PL enhancement and p-RTP features. These results not only provide a universal strategy for constructing efficient nonconventional luminophores but also shed new light on the underlying mechanism of biological autofluorescence.

INTRODUCTION

Nonconventional luminophores, lacking aromatic chromophores but possessing electron-rich moieties such as –NH_2,[1, 2] –OH,[3] –C=O[4], have garnered significant attention due to their promising applications in optoelectronic, biological, and medical fields.[5-7] These unique luminophores, often derive from natural products,[8] biomolecules,[9] and synthetic chemicals,[10, 11] generally exhibit excellent water solubility, low biotoxicity, and environmental friendliness.[5, 12] Their intrinsic photoluminescence (PL) can be explained by the clustering-triggered emission (CTE) mechanism, namely the PL arises from the clustering of electron-rich moieties, which leads to electron delocalization and conformational rigidity.[13-16] This enables intriguing PL characteristics, including aggregation-induced emission, excitation-dependent PL, and widespread phosphorescence.[17]

Nonaromatic amino acids, ubiquitous nonconventional luminophores in biological organisms, play a vital role in the PL of natural peptides[18] and proteins.[19] For instance, the light emission contributed by nonaromatic amino acids is often observed in amyloid-like proteins associated with neurodegenerative diseases.[6, 9, 20] Understanding their PL properties can aid in disease diagnosis and treatment.[21] Furthermore, the self-assembly of nonaromatic peptides can induce tunable intrinsic fluorescence, holding significant potential for nanotechnology applications.[22, 23] However, PL of nonaromatic amino acids is typically weak and primarily confined to the blue region, limiting their practical applications. Therefore, developing new efficient luminophores based on nonaromatic amino acids is essential. Nevertheless, a general and viable strategy for effectively enhancing the PL of nonaromatic amino acids while preserving excellent biocompatibility remains elusive. Critically, the lack of a comprehensive understanding of the fundamental causes of weak PL in nonaromatic amino acids significantly hinders our ability to design efficient luminescent systems.

Serendipitously, we found that glycosylating nonaromatic amino acids significantly enhances their PL, boosting both sugar and amino acid emission by up to 31-fold. For instance, glycosidic coupling of weakly emissive glucose (Glu) and L-Serine (Ser) results in GluSer crystals with high quantum yields (Φ_c) and remarkable persistent room temperature phosphorescence (p-RTP) (Figure 1). In contrast, the dimers of both compounds, *i.e.* cellobiose (disaccharides) and BSer (dipeptides) exhibit weak PL (Figure 1A,B), highlighting the crucial role of synergistic pairing of sugars and amino acids. Furthermore, this approach is testified universal and also allows for fine-tuning of the Φ_c, emission wavelengths (λ_{em}), and phosphorescence lifetimes (τ_p) by simply adjusting the types of sugars and amino acids used (Figure 1C). Herein, their PL behaviors and emissive mechanism were thoroughly investigated. This finding not only opens a new avenue for developing efficient luminophores, but also provides crucial insights into the underlying mechanisms of biological autofluorescence.[18, 19, 24, 25]

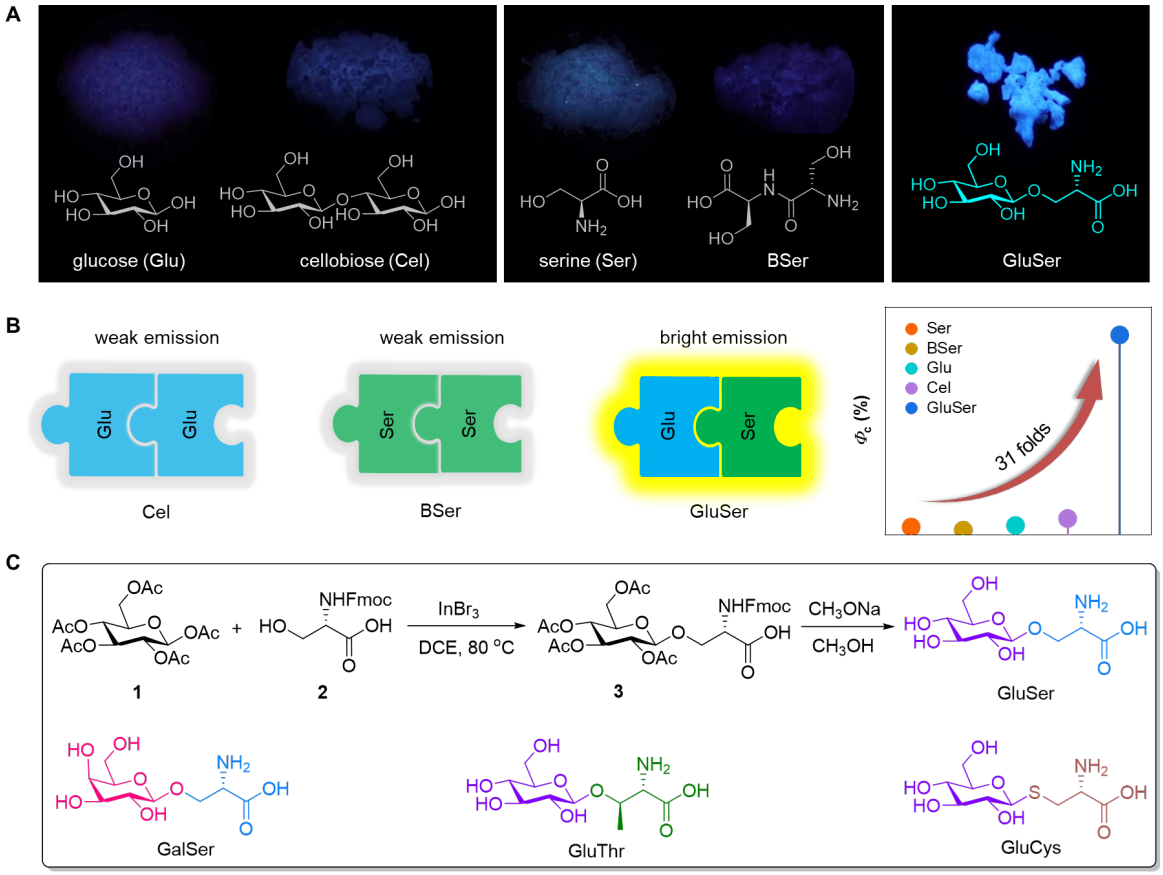

Figure 1. (A) Luminescent photographs taken under 312 nm UV light or after ceasing the irradiation. (B) Schematic illustration of the crystal emission and quantum yields (Φ_c) for the dimers of sugars and amino acids and their conjugates. (C) Synthetic route of GluSer and structures of other nonaromatic glycoamino acids studied herein.

RESULTS AND DISCUSSION

The target glycoamino acids were synthesized according to the procedures shown in Figure 1C. Notably, our initial attempts to link amino acids to glucose through their amino groups resulted in complex and unstable products, hindering their further purifications. Subsequently, we explored different coupling strategies, finding that the glycosidic bond formation yielded highly stable glycosylated amino acids. Briefly, taking GluSer as example, Fmoc-L-Serine **2** was glycosylated with β-glucose pentaacetate **1** using $InBr_3$ as a promoter to give compound **3**, followed by the removal of the 9-fluorenylmethoxycarbonyl (Fmoc) and acetyl protecting group with CH_3ONa in methanol, underwent two rounds of purification to furnish the resulting GluSer. The resulting compounds were thoroughly characterized by spectroscopy methods, including HPLC and $^1H/^{13}C$ NMR spectra (Figures S1–S5), testifying their high purity.

Under varying UV irradiation, Glu and Ser crystals exhibit weak bluish-violet luminescence, while GluSer crystals display bright blue emission (Figures 2A and S6), accompanying a significant increase in Φ_c, boosted 31-fold to 9.2% from merely 0.3% (Figure 2B). Both crystals and concentrated aqueous solutions (*e.g.* 0.1 M) of GluSer illustrate excitation-dependent emission (Figures 2C and S7). Specifically, with excitation wavelength (λ_{ex}) changing from 254 to 365 nm, the emission peaks and shoulders for GluSer crystals at 403/435/439/463/476 nm are noticed (Figure 2C), suggesting the presence of diversified emissive clusters. This is further supported by their distinct fluorescence lifetimes (τ_f) of 6.0/5.3/7.3 ns at 403/439/463 nm (Figure S8), respectively. In contrast to Glu and Ser crystals, GluSer crystals exhibit pronounced p-RTP emission, which is also λ_{ex}-dependent. After ceasing the 312 nm UV irradiation, a blueish-green afterglow lasting for over 4 s was observed (Figures 2A and S9). Adjusting the λ_{ex} from 254 to 365 nm, variable peaks ranging from blue to yellowish-green were recorded, accompanying distinct τ_p values (389~637 ms) and a dramatic redshift of ~70 nm (470~540 nm, Figure 2D), with the CIE (Commission Internationale de l'Eclairage) coordinates varying from (0.22, 0.26) to (0.33, 0.43) (Figure 2E). These results as well as the broad full width at half maximum (FWHM, 195~220 nm) of p-RTP further indicate the concurrence of heterogeneous emissive clusters in GluSer crystals. Above PL behaviors of GluSer crystals can be well understood by the CTE mechanism,[5] namely, the clustering of electron-rich moieties of oxygen, amine, and carboxyl groups results in diversified emissive species in GluSer crystals, which generate different emissions in response to the variation in λ_{ex}.

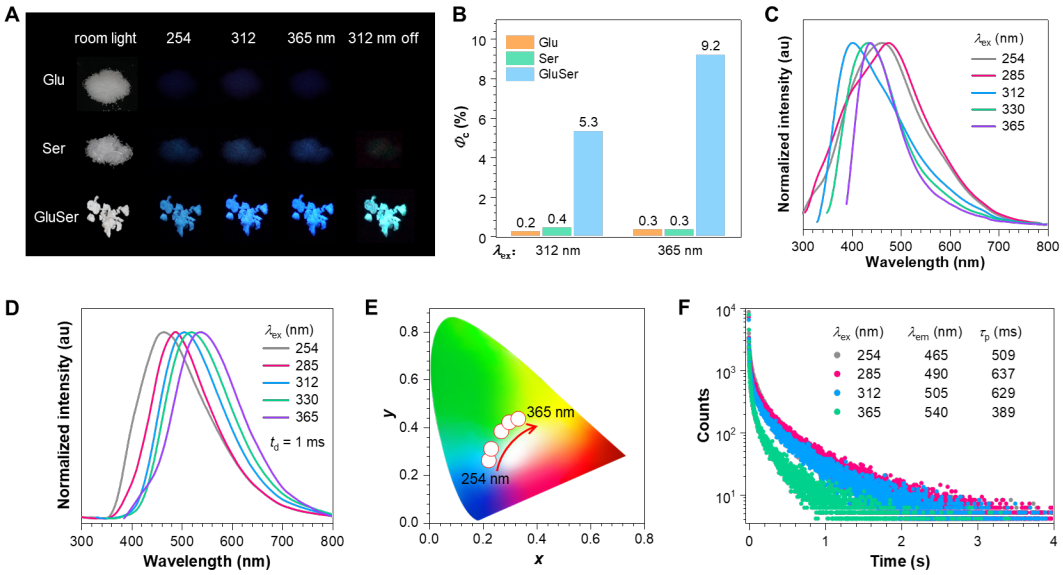

Figure 2. (A) Photographs of Glu, Ser, and GluSer crystals taken under room light, different UV lights, or after ceasing the 312 nm UV irradiation. (B) Φ_c of Glu, Ser, and GluSer. (C) Prompt and (D) delayed (t_d = 1 ms) emission spectra of GluSer crystals with different λ_{ex}s. (E) The CIE coordinate diagram of p-RTP for GluSer crystals with varying λ_{ex}s. (F) τ_p for GluSer crystals monitored at various λ_{em}s.

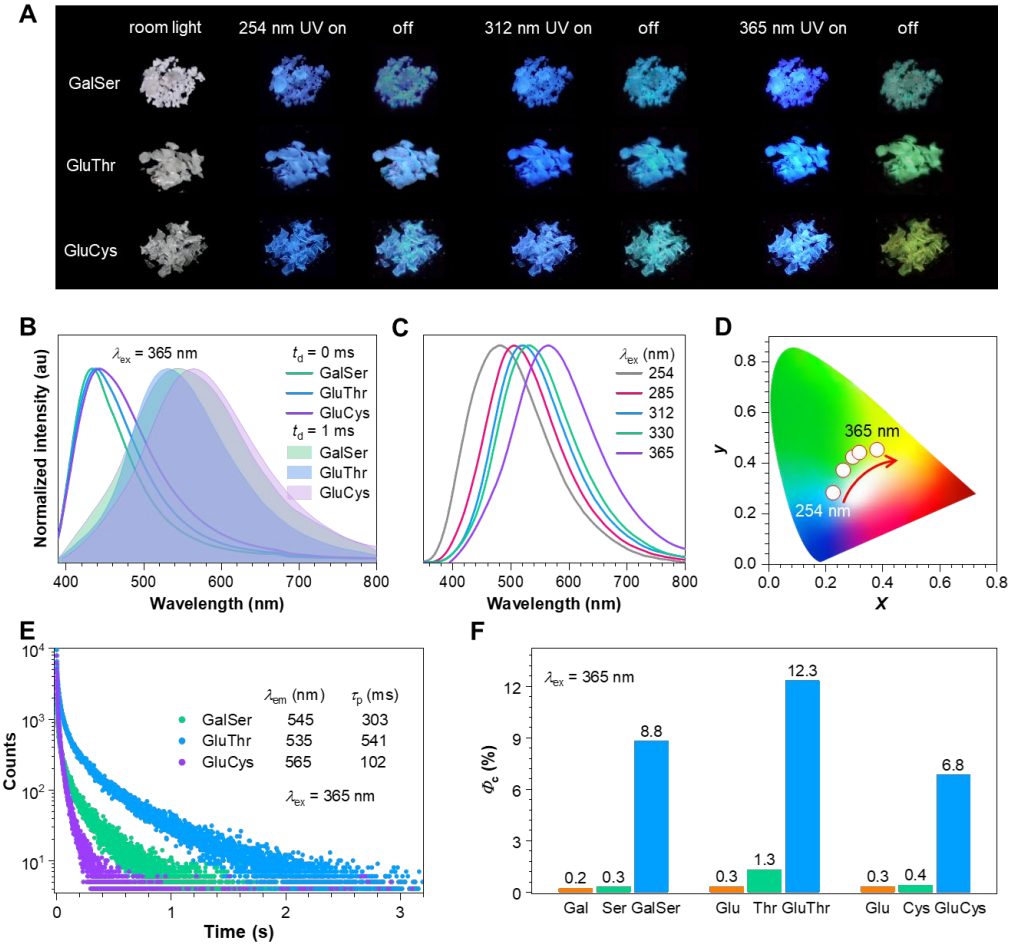

Figure 3. (A) Photographs of GalSer, GluTHr, and GluCys crystals taken under room light, different UV lights, or after ceasing the irradiation. (B) Prompt and delayed (t_d = 1 ms) PL spectra of varying crystals under 365 nm UV light. (C) Delayed (t_d = 1 ms) PL spectra and (D) CIE coordinate diagram with different λ_{ex}s for GluCys crystals. (E) τ_p and (F) Φ_c values of varying crystals.

To check whether such synergistic enhancement is universal or not, other glycoamino acids, GalSer, GluThr, and GluCys, were synthesized (Figure 1C and Schemes S1–S3). Distinct from the faint emission of corresponding sugars and amino acids, all above solids exhibit intense and excitation-dependent fluorescence and p-RTP (Figure 3A), which are consistent with those observed in GluSer crystals, thus testifying the universality of such synergistic PL enhancement. With 365 nm UV excitation, all crystals depict bright blue to cyan prompt PL and bluish-green to greenish-yellow p-RTP (Figure 3A,B). Specifically, GluCys crystals demonstrate red-shifted p-RTP (565 nm) with comparison to those of GalSer (545 nm) and GluThr (530 nm) crystals, which should be ascribed to the better electron-delocalization ability of the sulfur atom.[14, 26] Meanwhile, with the variation of λ_{ex} from 254 to 365 nm, the p-RTP peak of GluCys crystals is progressively adjusted from 480 to 565 nm (Figure 3C), achieving expanded tunable color from blue to greenish-yellow (Figures 3A,D and S10). Furthermore, the τ_p of different crystals is highly variable, which are 303, 542, and 102 ms for GalSer, GluThr, and GluCys crystals (Figure 3E, λ_{ex} = 365 nm), respectively. Notably, on account of the existence of diverse clusters, the τ_p also significantly varies at different emission peaks, which can even reach as long as 1020 ms (Figure S11). To further quantitatively evaluate the PL performance of these crystals, their Φ_cs were measured, which are 12.3%, 8.8%, and 6.8% for GluThr, GalSer and GluCys crystals (Figure 3F), respectively. These values are significantly higher, by orders of magnitude, than those of the corresponding sugars and amino acids alone, highlighting the robust and generalizable nature of this synergistic effect. Furthermore, the above results also strongly suggest the high potential for regulating PL and p-RTP colors, efficiencies, and lifetimes by adjusting the choice of sugars and/or amino acids.

To investigate the underlying mechanism for the glycosylation effect, we conducted a comprehensive study using GluSer as a representative model. Initial observations revealed a clear synergistic PL enhancement for GluSer compared to Glu and Ser individually. Cellobiose and BSer crystals, in sharp contrast, did not exhibit a significant increase in PL, with their Φ_c values remaining below 1% (Figures 1A,B and S12). These findings suggest that simple dimerization and enhanced electron distribution alone are insufficient for constructing efficient nonconventional luminophores. This indicates that the unique combination of Glu and Ser likely plays a crucial role in the synergistic effect.

To further elucidate the mechanism, we investigated the single-crystal structures and intermolecular interactions of the compounds. As depicted in Figures 4A and S13, multiple hydrogen bonds (C=O···H–N, C=O···H–O, H–O···H–O, etc.) as well as abundant short contacts (*e.g.* C=O···N–H, C=O···O–H, H–O···O–H) are found in Glu, Ser, and GluSer crystals. Notably, GluSer crystals demonstrate a more diversified interaction network of electron-rich functional groups, with the presence of additional C=O···O–H and H–O···N–H short contacts alongside those similar to Glu and Ser (H–O···O–H, C=O···N–H). Noncovalent interactions (NCI) analysis (Figure 4C) further highlights this enriched interaction network, revealing abundant through-space interactions (denoted pink area) between adjacent GluSer molecules, facilitating through-space conjugation (TSC). While both Ser and GluSer exist in zwitterionic form, the attraction between charged amino (NH_3^+) and carboxylate (COO^-) groups in GluSer is significantly stronger (Figure S14), suggesting a more compact molecular clustering.

Table 1. Dynamic photophysical parameters of the Glu, Ser and GluSer crystals.[a]

crystal	λ_f (nm)	λ_p (nm)	Φ_c (%)	Φ_f (%)	Φ_p (%)	τ_f (ns)	k_r^f (s^{-1})	k_{nr}^f (s^{-1})	τ_p (ms)	k_{isc} (s^{-1})	k_r^p (s^{-1})	k_{nr}^p (s^{-1})
Glu	375	510	0.2	0.16	0.04	5.1	3.1×10^5	2.0×10^8	115.2	7.8×10^4	3.5×10^{-3}	8.7
Ser	467	530	0.4	0.18	0.22	6.2	3.0×10^5	1.6×10^8	92.6	3.5×10^5	2.3×10^{-2}	10.8
GluSer	403	505	5.3	3.71	1.55	7.5	5.0×10^6	1.3×10^8	630.0	2.1×10^6	2.5×10^{-2}	1.6

[a] λ_{ex} = 312 nm; $\Phi_c = \Phi_f + \Phi_p$; $\Phi_{isc} = \Phi_p/(\Phi_p + \Phi_f)$; $k_{isc} = \Phi_{isc}\Phi_f/\langle\tau\rangle_f$; $k_r^p = \Phi_p/\tau_p$; $k_{nr}^p = (1-\Phi_p)/\tau_p$. λ_f and λ_p are the emission maxima of fluorescence and phosphorescence of the crystals. Φ_c, Φ_f, and Φ_p are the quantum efficiencies of total emission, fluorescence, and phosphorescence of the crystals, respectively.

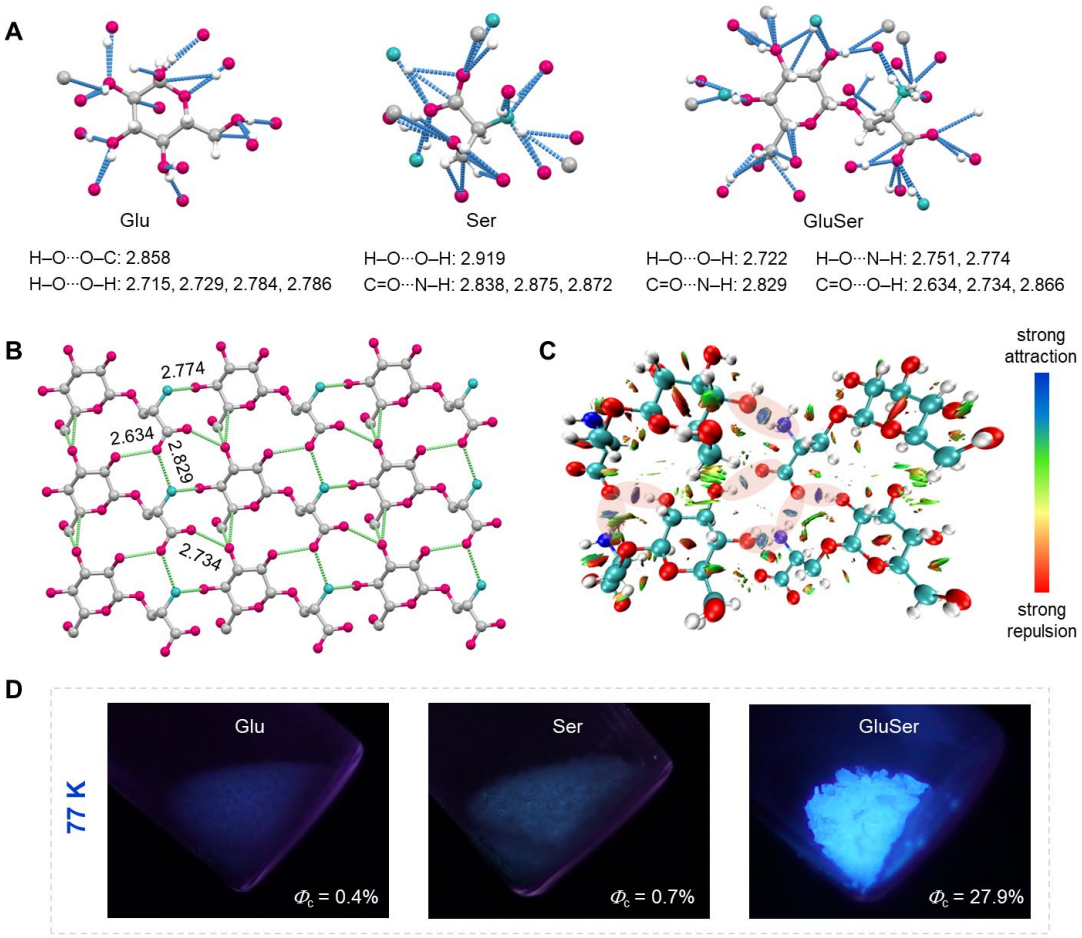

Figure 4. (A) Single-crystal structure with denoted intermolecular interactions of Ser, Glu, and GluSer. (B) Fragmental molecular packing with denoted short contacts among electron-rich units in GluSer. (C) NCI plots of GluSer. (D) Luminescent photographs of Glu, Ser, and GluSer crystals taken under 312 nm UV irradiation at 77 K.

It is noted that, previous literatures emphasized the importance of short hydrogen bonding or constraint stretching of carbonyl in amide groups, proposing the "carbonyl-lock" mechanism as the origin of the nonaromatic fluorescence.[24, 25] This insight prompts us to conduct a more detailed analysis and comparison of crystal packing and dynamic photophysical parameters. GluSer exhibits significantly stronger hydrogen bonding around the carbonyl group compared to Ser, and also displays a two-dimensional ordered arrangement (Figure 4B), which is absent in Glu and Ser crystals (Figure S13). This compact and orderly packing promotes a rigid conformation and restricts nonradiative dissipation, as evidenced by significantly reduced k_{nr} values for GluSer compared to Glu and Ser (Table 1), thus contributing to the enhanced PL.[27] However, the PL of Ser and Glu crystals remains weak even at 77 K, contrasting sharply with the remarkable enhancement observed in GluSer crystals, with the quantum yield increasing to 27.9% (Figure 4D). This indicates that mere rigidified conformation, which leads to the restriction of non-radiative transitions, is not the primary driver of the synergistic effect. Absorption measurement reveals an enhanced absorption at approximately 320 nm and a tail extending into the visible region for a 0.1 M aqueous solution of GluSer, compared to those of Glu and Ser (Figure S15), suggesting significantly extended electron delocalization in GluSer aggregates.[12] Therefore, we suppose that the synergistic effect is primarily attributed to the augmented absorption in GluSer, leading to more efficient excitation processes within the 280–400 nm range (Figure S15C). This hypothesis is further supported by the optimal λ_{ex} of Gluser crystals at 340 nm, in contrast to those of Ser and Glu crystals, which fall below 250 nm (Figure S15C).

Molecular electrostatic potential (ESP) analysis further supports our deductions. As illustrated in Figure 5A,B, only a slight accumulation of electrons is observed around the oxygen atoms of Glu. The ESP on the van der Waals (vdW) surface of the Glu dimer is distributed within a relatively narrow range of low values (–43.4 to 55.8 kcal/mol), indicating a relatively uniform electron distribution. In contrast, the ESP distribution of the Ser dimer is remarkably more polarized, ranging from –80.6 to 93.0 kcal/mol, suggesting charge separation within Ser, with electrons biased towards the COO^- moiety and positive charges distributed on the NH_3^+ unit. GluSer dimers exhibit a similar charge separation state, albeit weaker due to the mitigating influence of the electron-rich glucose moiety, resulting in a more homogeneous electron distribution. The inherent polarizing characteristic of Ser promotes electron mobility within and between molecules, leading to a more extensive spatial electron distribution, which is particularly evident in the ESP distribution of the GluSer tetramer (Figure S16). Furthermore, the presence of numerous electron-rich hydroxyl groups in Glu contributes to significant TSC in both Glu and GluSer, as indicated by the arrows in Figure 5A. Therefore, the binding of Glu and Ser

facilitates a more uniform electron distribution across a wider spatial range and promotes TSC, leading to extended overall electron delocalization and increased susceptibility to excitation in GluSer crystals.

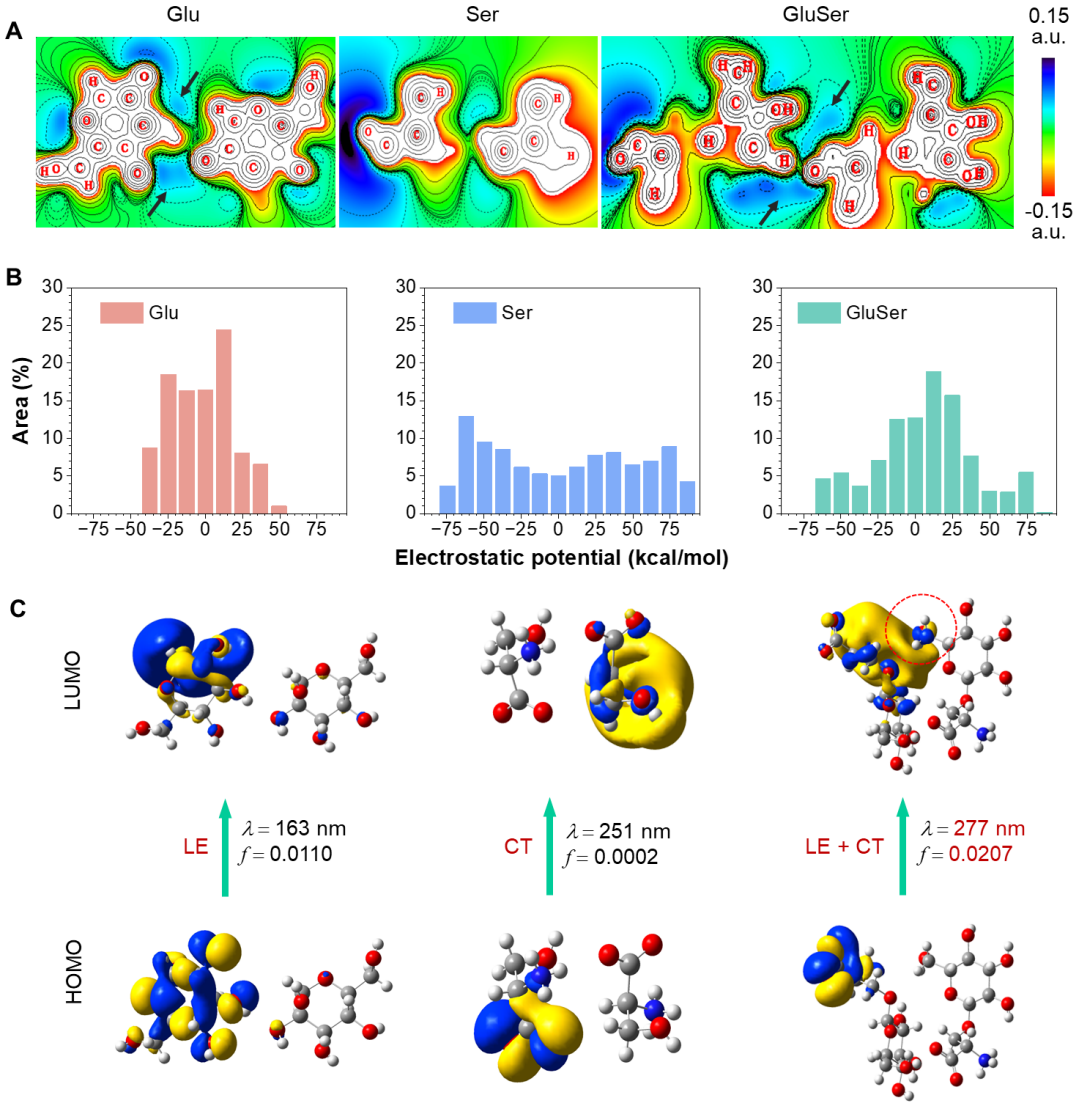

Figure 5. (A) Color-filled contour map of ESP and (B) surface area in each ESP range on the vdW surface for the dimers of Glu, Ser, and GluSer. Solid and dashed lines correspond to positive and negative regions, respectively. (C) HOMO and LUMO electron densities for Glu, Ser, and GluSer dimers.

To delve deeper into the mechanism underlying the synergistic effect, we employed ultrafast femtosecond transient absorption (fs-TA) spectroscopy to probe the excited-state properties of Glu, Ser, and GluSer. Unlike the nearly undetectable signals from Glu and Ser (Figure 6A,B), significant changes in the excited state of GluSer solution are observed in the fs-TA spectra following excitation at both 266 and 310 nm excitation (Figure 6C,D), further confirming the enhanced excitability of GluSer. After 266 nm excitation, the excited-state absorption (ESA) peak at 334 nm rapidly reaches to a maximum within 2.17 ps, followed by a gradual decline and red-shift to 348 nm within 18.5 ps (indicated by arrows in Figure 6D), suggesting the formation of a charge transfer (CT) state. This ESA peak at 348 nm can be attributed to the absorption of radical ions, corroborated by the red-shift in the PL emission of the GluSer solution with increasing solvent polarity (Figure S17).[28, 29] Subsequently, the ESA peak at 348 nm continues to decay, albeit at a much slower rate, with significant ESA signals still present at 6.86 ns, implying the remarkable stability of this CT state. Additionally, kinetic decay curve fitting using two exponential functions reveals lifetime parameters corresponding to the generation (τ_1) and decay (τ_2) of the CT state (Figure 6E). According to the kinetic decay curve of nanosecond transient absorption (ns-TA) (Figure 6F), the ESA peak at 379 nm decays under oxygen similar that in a nitrogen atmosphere, with very similar decay lifetimes (Figure S18), indicative of the singlet nature of this CT state. Notably, upon excitation at 310 nm, a similar evolution of the excited state is observed (Figure 6C), further emphasizing the characteristic CT behavior in the excited state of GluSer.

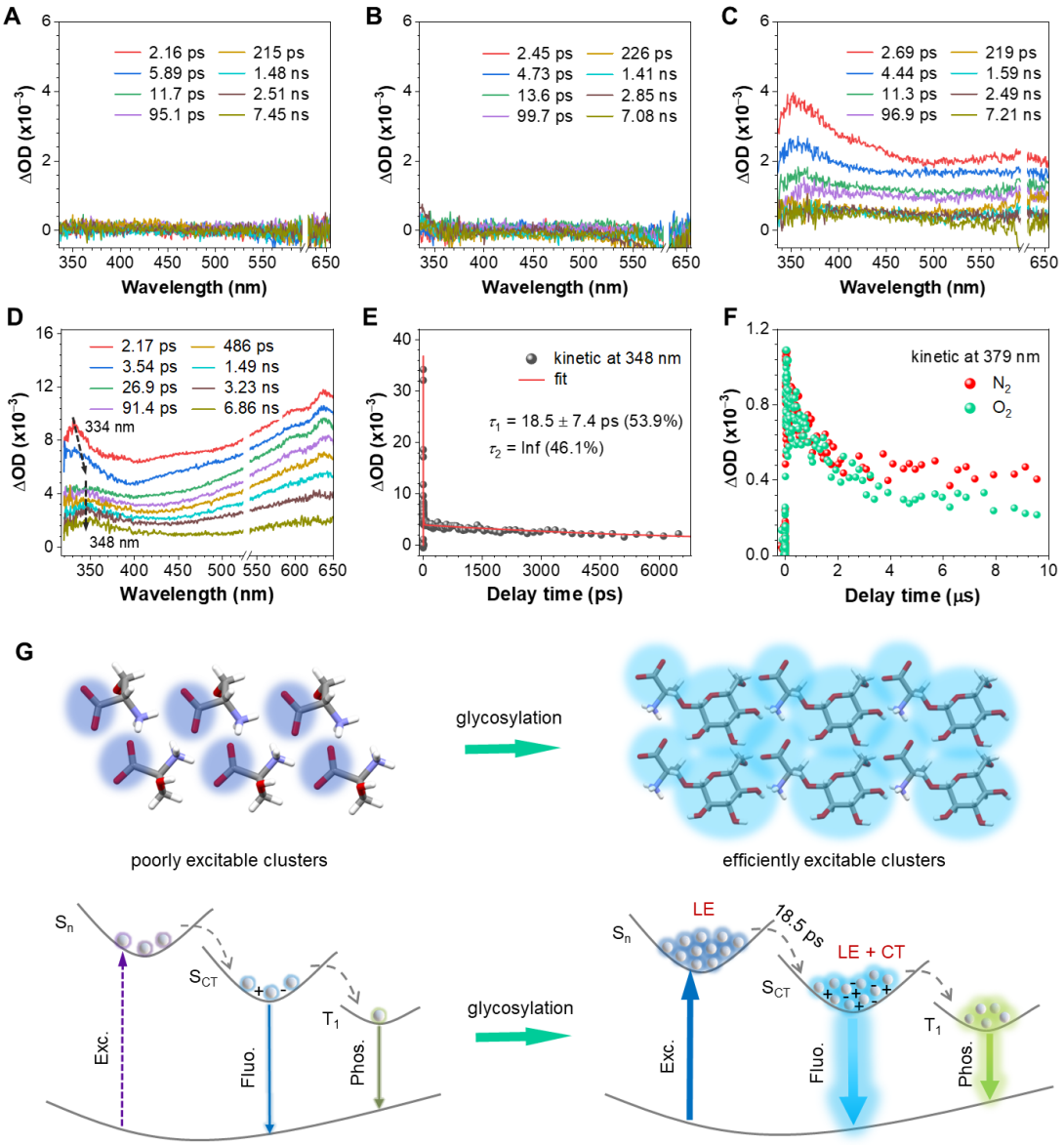

Figure 6. (A–C) The ultrafast femtosecond transient absorption (fs-TA) spectra of 1 M aqueous solutions of (A) Glu, (B) Ser, and (C) GluSer after 310 nm excitation. (D) The fs-TA spectra and (E) the decay curve in 348 nm of 1 M GluSer aqueous solution after 266 nm excitation. (F) The ns-TA spectra decay curve of 1 M GluSer aqueous solution under N_2 and O_2 atmosphere. (G) Proposed mechanism of the synergistic PL enhancement effect.

To gain further insights into the excited-state properties, we performed time-dependent density functional theory (TD-DFT) calculations. As shown in Figure 5C, the electron distribution of HOMO and LUMO levels in Glu dimer demonstrates substantial overlap, indicative of a predominant locally excited (LE) character. However, this limited electron delocalization results in a high energy gap (6.3305 eV, 195.9 nm), making excitation highly challenging. Consequently, Glu crystals exhibit only faint blue-violet emission under UV irradiation (Figures 2A and S6). In contrast, the excited state of the Ser dimer displays a distinct CT character, leading to a much lower energy gap (Figure 5C).[30-32] Nevertheless, the oscillator strength of Ser dimer (f = 0.0002) is significantly lower than that of Glu dimer (f = 0.0110), because of the minimal overlap between its HOMO and LUMO,[33] hindering efficient excitation and resulting in faint blue emission (Figures 2A and S6).

Interestingly, combining Glu and Ser leads to a notable attenuation of the CT characteristic in GluSer compared to that of Ser (Figure 5C) while simultaneously introducing an LE component. This brings about intensive TSC amongst the amino and hydroxyls on the LUMOs (Figure 5C), likely due to moderate charge separation. The natural transition orbitals (NTO) analysis also reveals similar transition modes and electron distribution characteristics (Figure S19). Consequently, the energy gap of GluSer dimer is effectively reduced while maintaining a higher oscillator strength,[34, 35] and the hybrid LE and CT state effectively increases the k_r (Table 1),[36] thus significantly enhances the PL performance of GluSer (Figures 2B and 5C). Furthermore, the involvement of CT narrows the energy gap between the first singlet and triplet excited states (ΔE_{ST}) in GluSer, facilitating intersystem crossing (ISC) and subsequent p-RTP emission,[37 38] which leads to a notable enhancement in k_{isc} and Φ_p. (Figure 5C, Table 1). Therefore, the

hybridization of LE and CT in GluSer serves as a key factor driving the synergistic effect. Above results clearly suggest that the synergistic combination of Ser and Glu not only promotes extended electron delocalization through a wider, more uniform electron distribution but also introduces hybrid LE and CT features, ultimately leading to significantly enhanced emission (Figure 6G).

CONCLUSIONS

In conclusion, glycosylation of nonaromatic amino acids is found effective to strikingly boosts the PL performance of both sugars and amino acids by a magnitude order (up to 31-fold). The intrinsic emission of corresponding sugars and amino acids is inherently weak due to their poor absorption and limited excitation propensity. Upon combination, the electron-rich glucose moiety enhances the electron abundance, mitigating the extreme charge distribution of the amino acids. Concurrently, the charge separation within the nonaromatic amino acids redistributes electrons in the oxygen clusters of the sugar moieties, effectively promoting electron delocalization, leading to enhanced absorption and excitation.

This synergistic approach is proven universal and moreover can be utilized to regulate the PL properties (*e.g.* color, efficiency) of the resulting crystals through flexible combination of different sugars and amino acids. The fs-TA and ns-TA spectroscopy, coupled with theoretical calculations, further underscore the importance of the hybrid LE and CT state in augmenting PL and promoting p-RTP features. This marks the inaugural report of synergistically boosted PL in nonconventional luminophores via the hybridization of LE and CT states, thereby offering fresh design principles for constructing efficient nonconventional luminophores and laying the theoretical groundwork for comprehending the autofluorescence in biological substances.

ASSOCIATED CONTENT

Supporting Information

Experimental details, characterizations, crystallographic information, PL spectra, and theoretical calculation details (PDF)

AUTHOR INFORMATION

Corresponding Author

Wang Zhang Yuan – *School of Chemistry and Chemical Engineering, Frontiers Science Center for Transformative Molecules, Shanghai Jiao Tong University, No. 800 Dongchuan Rd., Minhang District, Shanghai 200240, China;* orcid.org/0000-0001-6340-3497; Email: wzhyuan@sjtu.edu.cn

Authors

Qiang Zhang – *School of Chemistry and Chemical Engineering, Frontiers Science Center for Transformative Molecules, Shanghai Jiao Tong University, No. 800 Dongchuan Rd., Minhang District, Shanghai 200240*

Zihao Zhao – *School of Chemistry and Chemical Engineering, Frontiers Science Center for Transformative Molecules, Shanghai Jiao Tong University, No. 800 Dongchuan Rd., Minhang District, Shanghai 200240*

Guanxin Yang – *School of Chemistry and Chemical Engineering, Frontiers Science Center for Transformative Molecules, Shanghai Jiao Tong University, No. 800 Dongchuan Rd., Minhang District, Shanghai 200240*

Anze Li – *School of Chemistry and Chemical Engineering, Frontiers Science Center for Transformative Molecules, Shanghai Jiao Tong University, No. 800 Dongchuan Rd., Minhang District, Shanghai 200240*

Yijing Cui – *School of Chemistry and Chemical Engineering, Frontiers Science Center for Transformative Molecules, Shanghai Jiao Tong University, No. 800 Dongchuan Rd., Minhang District, Shanghai 200240*

Yusong Cai – *School of Chemistry and Chemical Engineering, Frontiers Science Center for Transformative Molecules, Shanghai Jiao Tong University, No. 800 Dongchuan Rd., Minhang District, Shanghai 200240*

Zhuojie Yin – *School of Chemistry and Chemical Engineering, Frontiers Science Center for Transformative Molecules, Shanghai Jiao Tong University, No. 800 Dongchuan Rd., Minhang District, Shanghai 200240*

Yuntian Tan – *Shanghai High School, No. 400 Shangzhong Rd., Xuhui District, Shanghai 200231, China*

Chenyang Zhou – *High School Affiliated to Shanghai Jiao Tong University, No.68 Yingao Rd., Yangpu District, Shanghai 200439, China*

Qian Peng – *School of Chemical Sciences, University of Chinese Academy of Sciences, Beijing 100049, China*

CONFLICTS OF INTERE

The authors declare no competing financial interest.

ACKNOWLEDGMENT

This work was financially supported by the National Natural Science Foundation of China (U22A20250 and 52073172).

REFERENCES

(1) Wang, D.; Imae, T. Fluorescence Emission from Dendrimers and Its pH Dependence. *J. Am. Chem. Soc.* **2004**, *126* (41), 13204–13205.

(2) Fan, Q.; Tang, Y.; Sun, H.; Guo, D.; Ma, J.; Guo, J. Cluster-Triggered Self-Luminescence, Rapid Self-Healing, and Adaptive Reprogramming Liquid Crystal Elastomers Enabled by Dynamic Imine Bond. *Adv. Mater.* **2024**. DOI: 10.1002/adma.202401315.

(3) Lee, W. I.; Bae, Y.; Bard, A. J. Strong Blue Photoluminescence and ECL from OH-Terminated PAMAM Dendrimers in the Absence of Gold Nanoparticles. *J. Am. Chem. Soc.* **2004**, *126* (27), 8358–8359.

(4) Shi, C. Y.; He, D. D.; Wang, B. S.; Zhang, Q.; Tian, H.; Qu, D. H. A Dynamic Supramolecular H-bonding Network with Orthogonally Tunable Clusteroluminescence. *Angew. Chem. Int. Ed.* **2023**, *62* (3), e202214422.

(5) Tang, S.; Yang, T.; Zhao, Z.; Zhu, T.; Zhang, Q.; Hou, W.; Yuan, W. Z. Nonconventional Luminophores: Characteristics, Advancements and Perspectives. *Chem. Soc. Rev.* **2021**, *50* (22), 12616–12655.

(6) Pansieri, J.; Josserand, V.; Lee, S.-J.; Rongier, A.; Imbert, D.; Sallanon, M. M.; Kövari, E.; Dane, T. G.; Vendrely, C.; Chaix-Pluchery, O.; Guidetti, M.; Vollaire, J.; Fertin, A.; Usson, Y.; Rannou, P.; Coll, J.-L.; Marquette, C.; Forge, V. Ultraviolet–Visible–Near-Infrared optical Properties of Amyloid Fibrils Shed Light on Amyloidogenesis. *Nat. Photon.* **2019**, *13* (7), 473–479.
(7) Wu, J.; Wang, Y.; Jiang, P.; Wang, X.; Jia, X.; Zhou, F. Multiple Hydrogen-Bonding Induced Nonconventional Red Fluorescence Emission in Hydrogels. *Nat. Commun.* **2024**, *15* (1), 3482.
(8) Cai, S.; Sun, Z.; Wang, H.; Yao, X.; Ma, H.; Jia, W.; Wang, S.; Li, Z.; Shi, H.; An, Z.; Ishida, Y.; Aida, T.; Huang, W. Ultralong Organic Phosphorescent Foams with High Mechanical Strength. *J. Am. Chem. Soc.* **2021**, *143* (39), 16256–16263.
(9) Pinotsi, D.; Grisanti, L.; Mahou, P.; Gebauer, R.; Kaminski, C. F.; Hassanali, A.; Kaminski Schierle, G. S. Proton Transfer and Structure-Specific Fluorescence in Hydrogen Bond-Rich Protein Structures. *J. Am. Chem. Soc.* **2016**, *138* (9), 3046–3057.
(10) Chu, B.; Liu, X.; Li, X.; Zhang, Z.; Sun, J. Z.; Yang, Q.; Liu, B.; Zhang, H.; Zhang, C.; Zhang, X. H. Phosphine-Capped Effects Enable Full-Color Clusteroluminescence in Nonconjugated Polyesters. *J. Am. Chem. Soc.* **2024**, *146* (15), 10889–10898.
(11) Li, H.; Gu, J.; Wang, Z.; Wang, J.; He, F.; Li, P.; Tao, Y.; Li, H.; Xie, G.; Huang, W.; Zheng, C.; Chen, R. Single-Component Color-Tunable Circularly Polarized Organic Afterglow Through Chiral Clusterization. *Nat. Commun.* **2022**, *13* (1), 429.
(12) Zhang, H.; Tang, B. Z. Through-Space Interactions in Clusteroluminescence. *JACS Au* **2021**, *1* (11), 1805–1814.
(13) Zhao, Z.; Cai, Y.; Zhang, Q.; Li, A.; Zhu, T.; Chen, X.; Yuan, W. Z. Photochromic Luminescence of Organic Crystals Arising from Subtle Molecular Rearrangement. *Nat. Commun.* **2024**, *15* (1), 5054.
(14) Zhu, T.; Yang, T.; Zhang, Q.; Yuan, W. Z. Clustering and Halogen Effects Enabled Red/Near-Infrared Room Temperature Phosphorescence from Aliphatic Cyclic Imides. *Nat. Commun.* **2022**, *13* (1), 2658.
(15) Zhang, X.; Bai, Y.; Deng, J.; Zhuang, P.; Wang, H. Effects of Nonaromatic Through-Bond Conjugation and Through-Space Conjugation on the Photoluminescence of Nontraditional Luminogens. *Aggregate* **2024**, *5* (3), e517.
(16) He, Y.; Feng, W.; Qiao, Y.; Tian, Z.; Tang, B. Z.; Yan, H. Hyperbranched Polyborosiloxanes: Non-traditional Luminescent Polymers with Red Delayed Fluorescence. *Angew. Chem. Int. Ed.* **2023**, *62* (48), e202312571.
(17) Ren, Y.; Dai, W.; Guo, S.; Dong, L.; Huang, S.; Shi, J.; Tong, B.; Hao, N.; Li, L.; Cai, Z.; Dong, Y. Clusterization-Triggered Color-Tunable Room-Temperature Phosphorescence from 1,4-Dihydropyridine-Based Polymers. *J. Am. Chem. Soc.* **2022**, *144* (3), 1361–1369.
(18) Chen, X.; Luo, W.; Ma, H.; Peng, Q.; Yuan, W. Z.; Zhang, Y. Prevalent Intrinsic Emission from Nonaromatic Amino Acids and Poly(amino acids). *Sci. China Chem.* **2017**, *61* (3), 351–359.
(19) Wang, Q.; Dou, X.; Chen, X.; Zhao, Z.; Wang, S.; Wang, Y.; Sui, K.; Tan, Y.; Gong, Y.; Zhang, Y.; Yuan, W. Z. Reevaluating Protein Photoluminescence: Remarkable Visible Luminescence upon Concentration and Insight into the Emission Mechanism. *Angew. Chem. Int. Ed.* **2019**, *58* (36), 12667–12673.
(20) Chan, F. T.; Kaminski Schierle, G. S.; Kumita, J. R.; Bertoncini, C. W.; Dobson, C. M.; Kaminski, C. F. Protein Amyloids Develop an Intrinsic Fluorescence Signature During Aggregation. *Analyst* **2013**, *138* (7), 2156–2162.
(21) Stower, H. Searching for Alzheimer's disease therapies. *Nat. Med.* **2018**, *24* (7), 894-897.
(22) Handelman, A.; Lapshina, N.; Apter, B.; Rosenman, G. Peptide Integrated Optics. *Adv. Mater.* **2018**, *30* (5), 1705776.
(23) Liao, P.; Zang, S.; Wu, T.; Jin, H.; Wang, W.; Huang, J.; Tang, B. Z.; Yan, Y. Generating Circularly Polarized Luminescence from Clusterization-Triggered Emission Using Solid Phase Molecular Self-assembly. *Nat. Commun.* **2021**, *12* (1), 5496.
(24) Stephens, A. D.; Qaisrani, M. N.; Ruggiero, M. T.; Diaz Miron, G.; Morzan, U. N.; Gonzalez Lebrero, M. C.; Jones, S. T. E.; Poli, E.; Bond, A. D.; Woodhams, P. J.; Kleist, E. M.; Grisanti, L.; Gebauer, R.; Zeitler, J. A.; Credgington, D.; Hassanali, A.; Kaminski Schierle, G. S. Short Hydrogen Bonds Enhance Nonaromatic Protein-related Fluorescence. *Proc. Natl Acad. Sci. USA* **2021**, *118* (21), e2020389118.
(25) Miron, G. D.; Semelak, J. A.; Grisanti, L.; Rodriguez, A.; Conti, I.; Stella, M.; Velusamy, J.; Seriani, N.; Doslic, N.; Rivalta, I.; Garavelli, M.; Estrin, D. A.; Kaminski Schierle, G. S.; Gonzalez Lebrero, M. C.; Hassanali, A.; Morzan, U. N. The Carbonyl-Lock Mechanism Underlying Non-aromatic Fluorescence in Biological Matter. *Nat. Commun.* **2023**, *14* (1), 7325.
(26) Zhang, T.; Ma, X.; Wu, H.; Zhu, L.; Zhao, Y.; Tian, H. Molecular Engineering for Metal-Free Amorphous Materials with Room-Temperature Phosphorescence. *Angew. Chem. Int. Ed.* **2020**, *59* (28), 11206–11216.
(27) Liang, Y.; Xu, C.; Zhang, H.; Wu, S.; Li, J. A.; Yang, Y.; Mao, Z.; Luo, S.; Liu, C.; Shi, G.; Sun, F.; Chi, Z.; Xu, B. Color-Tunable Dual-Mode Organic Afterglow from Classical Aggregation-Caused Quenching Compounds for White-Light-Manipulated Anti-Counterfeiting. *Angew. Chem. Int. Ed.* **2023**, *62* (7), e202217616.
(28) Yao, L.; Zhang, S.; Wang, R.; Li, W.; Shen, F.; Yang, B.; Ma, Y. Highly Efficient Near-Infrared Organic Light-Emitting Diode Based on a Butterfly-Shaped Donor-Acceptor Chromophore with Strong Solid-State Fluorescence and a Large Proportion of Radiative Excitons. *Angew. Chem. Int. Ed.* **2014**, *53* (8), 2119-2123.
(29) Huang, W.; Zhang, X.; Su, H.; Zhang, B.; Feng, A.; Jiang, J.; Chen, B.; Zhang, G. Trapping Highly Reactive Photoinduced Charge-Transfer Complex Between Amine and Imide by Light. *Chem*. **2024**. DOI: 10.1016/j.chempr.2024.05.005.
(30) Prasad, S.; Mandal, I.; Singh, S.; Paul, A.; Mandal, B.; Venkatramani, R.; Swaminathan, R. Near UV-Visible Electronic Absorption Originating from Charged Amino Acids in a Monomeric Protein. *Chem. Sci.* **2017**, *8* (8), 5416–5433.
(31) Mandal, I.; Manna, S.; Venkatramani, R. UV-Visible Lysine-Glutamate Dimer Excitations in Protein Charge Transfer Spectra: TDDFT Descriptions Using an Optimally Tuned CAM-B3LYP Functional. *J. Phys. Chem. B* **2019**, *123* (51), 10967–10979.
(32) Yang, G.; Hao, S.; Deng, X.; Song, X.; Sun, B.; Hyun, W. J.; Li, M. D.; Dang, L. Efficient Intersystem Crossing and Tunable Ultralong Organic Room-Temperature Phosphorescence via Doping Polyvinylpyrrolidone with Polyaromatic Hydrocarbons. *Nat. Commun.* **2024**, *15* (1), 4674.
(33) Li, S.; Chen, J.; Wei, Y.; De, J.; Geng, H.; Liao, Q.; Chen, R.; Fu, H. An Organic Laser Based on Thermally Activated Delayed Fluorescence with Aggregation-Induced Emission and Local Excited State Characteristics. *Angew. Chem. Int. Ed.* **2022**, *61* (39), e202209211.
(34) Gao, Y.; Zhang, S.; Pan, Y.; Yao, L.; Liu, H.; Guo, Y.; Gu, Q.; Yang, B.; Ma, Y. Hybridization and de-Hybridization Between the Locally-Excited (LE) State and the Charge-Transfer (CT) State: a Combined Experimental and Theoretical Study. *Phys. Chem. Chem. Phys.* **2016**, *18* (35), 24176–24184.
(35) Li, W.; Pan, Y.; Xiao, R.; Peng, Q.; Zhang, S.; Ma, D.; Li, F.; Shen, F.; Wang, Y.; Yang, B.; Ma, Y. Employing ∼100% Excitons in OLEDs by Utilizing a Fluorescent Molecule with Hybridized Local and Charge-Transfer Excited State. *Adv. Funct. Mater.* **2013**, *24* (11), 1609–1614.
(36) Gould, I. R.; Young, R. H.; Mueller, L. J.; Albrecht, A. C.; Farid, S. Electronic Structures of Exciplexes and Excited Charge-Transfer Complexes. *J. Am. Chem. Soc.* **1994**, *116* (18), 8188–8199.
(37) Chen, H.; Hou, Y.; Shi, Y.; Zhang, Y.; Wang, S.; Peng, Q.; Huang, H. Organic All-Photonic Artificial Synapses Enabled by Anti-Stokes Photoluminescence. *J. Am. Chem. Soc.* **2023**, *145* (22), 11988–11996.
(38) Li, D.; Yang, Y.; Yang, J.; Fang, M.; Tang, B. Z.; Li, Z. Completely Aqueous Processable Stimulus Responsive Organic Room Temperature Phosphorescence Materials with Tunable Afterglow Color. *Nat. Commun.* **2022**, *13* (1), 347.

TOC Graphic